

A SPECTROSCOPIC SEARCH FOR LEAKING LYMAN CONTINUUM AT $Z \sim 0.7^{\dagger}$

CARRIE R. BRIDGE¹, HARRY I. TEPLITZ², BRIAN SIANA¹, CLAUDIA SCARLATA³, GWEN C. RUDIE¹, JAMES COLBERT³, HENRY C. FERGUSON⁴, THOMAS M. BROWN⁴, CHRISTOPHER J. CONSELICE⁵, LEE ARMUS³, MARA SALVATO^{1,10}, DULIA F. DE MELLO⁶, MARK DICKINSON⁷, JONATHAN P. GARDNER⁸, MAURO GIAVALISCO⁴

Draft version February 12, 2010

ABSTRACT

We present the results of rest-frame, UV slitless spectroscopic observations of a sample of 32 $z \sim 0.7$ Lyman Break Galaxy (LBG) analogs in the COSMOS field. The spectroscopic search was performed with the Solar Blind Channel (SBC) on *HST*. While we find no direct detections of the Lyman Continuum we achieve individual limits (3σ) of the observed non-ionizing UV to Lyman continuum flux density ratios, $f_{\nu}(1500\text{\AA})/f_{\nu}(830\text{\AA})$ of 20 to 204 (median of 73.5) and 378.7 for the stack. Assuming an intrinsic Lyman Break of 3.4 and an optical depth of Lyman continuum photons along the line of sight to the galaxy of 85% we report an upper limit for the *relative* escape fraction in individual galaxies of 0.02 – 0.19 and a stacked 3σ upper limit of 0.01. We find no indication of a relative escape fraction near unity as seen in some LBGs at $z \sim 3$. Our UV spectra achieve the deepest limits to date at any redshift on the escape fraction in individual sources. The contrast between these $z \sim 0.7$ low escape fraction LBG analogs with $z \sim 3$ LBGs suggests that either the processes conducive to high f_{esc} are not being selected for in the $z \lesssim 1$ samples or the average escape fraction is decreasing from $z \sim 3$ to $z \sim 1$. We discuss possible mechanisms which could affect the escape of Lyman continuum photons.

Subject headings: cosmology: observations — galaxies: evolution — ultraviolet: galaxies

1. INTRODUCTION

Reionization brought an end to the cosmic “dark ages,” during which the Universe contained a mostly neutral intergalactic medium (IGM). This transition is thought to be triggered by either the radiation from QSOs or from galaxies containing large populations of massive stars. Recent determinations of the high redshift QSO luminosity function suggest that QSO space densities are too low to reionize the universe at $z > 6$ (Siana et al. 2008; Jiang et al. 2008). The contribution of galaxies to the ionizing UV background (Madau et al. 1999) depends upon how many of the Lyman Continuum (LyC) photons produced by massive young stars that are not absorbed

by neutral Hydrogen atoms or dust grains. Direct measurement of the escape fraction, f_{esc} , is impossible at the epoch of reionization, because intervening absorbers make the IGM opaque to LyC photons. Instead, f_{esc} must be measured at lower redshifts ($z \lesssim 3.5$) in objects that are analogous to the galaxies responsible for reionization.

Detection of escaping LyC photons has eluded most surveys. Observations of Lyman Break Galaxies (LBGs) at $z \sim 3$ (Steidel et al. 2001; Shapley et al. 2006; Iwata et al. 2009) suggest that in $\sim 10\%$ of starbursts the escape fraction is quite large, nearing unity. In contrast, there are currently no LyC detections locally ($z \lesssim 1$), despite tremendous effort (Leitherer et al. 1995; Giallongo et al. 1997; Deharveng et al. 2001; Malkan et al. 2003; Siana et al. 2007; Cowie et al. 2008, see Siana et al. 2010 for a review). One explanation suggested by several authors is the cosmic average escape fraction evolves with redshift (Inoue et al. 2006; Siana et al. 2007, 2010). One notable difference between high and low redshift studies of the escape fraction is the wavelength range used to measure the LyC flux. All previous surveys searching for intermediate redshift LyC leaking galaxies have utilized broad-band photometry which probe $\sim 700\text{\AA}$ while ~ 3 studies measure the LyC just below the Lyman limit. Probing these shorter wavelengths increases the sensitivity to the star formation history. Meaning a decrease in star formation within the last 10 Myr would significantly lower the flux at 700\AA compared to 900\AA weakening the LyC limits measured from broad-band photometry. With this difference in mind and we have undertaken a large spectroscopic program with the *Hubble Space Telescope* (HST) to study the escape fraction in luminous starbursts at $z \sim 0.7$ (GO 11236; PI=Teplitz).

Using the Solar Blind Channel (SBC) of the Advanced Camera for Surveys (ACS), we have obtained

¹ California Institute of Technology, 220-6, Pasadena, CA 91125
² Infrared Processing and Analysis Center, MS 100-22, Caltech, Pasadena, CA 91125

³ Spitzer Science Center, California Institute of Technology, 220-6, Pasadena, CA 91125

⁴ Space Telescope Science Institute, 3700 San Martin Drive, Baltimore, MD 21218

⁵ University of Nottingham, Nottingham, NG7 2RD, UK

⁶ Department of Physics, Catholic University of America, 620 Michigan Avenue, Washington DC 20064

⁷ National Optical Astronomy Observatory, 950 N. Cherry Ave., Tucson, AZ 85719

⁸ Exploration of the Universe Division, Observational Cosmology Laboratory, Code 665, Goddard Space Flight Center, Greenbelt, MD 20771

⁹ Department of Physics and Astronomy, Rutgers University, 136 Frelinghuysen Road, Piscataway, NJ 08854

¹⁰ Max-Planck institute for Plasma Physics & Excellence Cluster Boltzmanns strasse 2, Garching 86748 Germany

[†] Based on observations made with the NASA/ESA Hubble Space Telescope, obtained at the Space Telescope Science Institute, which is operated by the Association of Universities for Research in Astronomy, Inc., under NASA contract NAS 5-26555. These observations are associated with programs 7410, 9478, and 10403 (HDF-WFPC2, 7817 HDF-NICMOS, 9978,10086 UDF-ACS,9803 UDF-NICMOS).

Electronic address: bridge@ipac.caltech.edu

far-ultraviolet (FUV) spectra of 32 starbursts chosen to be good analogs of LBGs. The observations presented in this paper cover rest-frame $\sim 750\text{--}1100 \text{\AA}$, and provide the first spectroscopic search for LyC photons from galaxies at $0 < z < 3$, as well as the deepest limits on the escape fraction for individual galaxies at any redshift. Slitless spectroscopy not only has an advantage over broad-band imaging by being able to probe closer to the Lyman limit (up to 880\AA vs. 700\AA), but its high spatial resolution makes it possible to study any offset of LyC radiation compared to UV emission. The large sample size provides enough number statistics to make a meaningful comparison with the rare LBG detections.

While no LyC photons are conclusively detected, we use these spectra to place strict limits on the UV ($\sim 1025\text{\AA}$) to Lyman continuum ($780 - 860\text{\AA}$) ratio and infer the limit on the escape fraction of ionizing photons. In section 2, we describe the selection of LBG-analog targets; in section 3, we present the observations and data reduction. The method of measuring limits on the escape fraction is presented in section 4. In sections 5 and 6, we give the results and discuss their implications. A cosmology of $\Omega_M = 0.3$, $\Omega_\Lambda = 0.70$, and $H_0 = 70 \text{ km s}^{-1} \text{ Mpc}^{-1}$ is assumed throughout.

2. SAMPLE SELECTION

Our aim was to choose galaxies at moderate redshift which are analogs of the high redshift starbursts postulated to be responsible for reionization. The better studied $z \sim 3$ LBG population is conventionally taken as accessible analogs to $z > 6$ galaxies. However, analogs at even lower redshift provide the opportunity for a wide range of observations, together with the opportunity to study the possible evolution of the escape fraction with redshift. Hoopes et al. (2007) demonstrated the similarity between LBGs and the compact subset of local UV Luminous Galaxies (UVLG Heckman et al. 2005). These sources share many properties with LBGs including luminosity, size, specific star-formation rate, mass, and metallicity. The compact UVLG population is quite rare locally (about 1 per square degree at $z < 0.3$), but its numbers increase with redshift. They are identified by their UV luminosity ($> 10^{10} L_\odot$) and surface brightness ($I_{FUV} > 10^8 L_\odot \text{ kpc}^{-2}$) Hoopes et al. (2007).

The wavelength range of the SBC/PR130L configuration limits the redshift range in which we can measure the LyC to $0.6 < z < 0.85$. Furthermore, SBC prism spectra are slitless, introducing a smearing effect, whereby the spectral resolution is degraded proportional to the spatial extent of the target. Thus, we were further restricted our selection to compact galaxies.

To choose appropriate targets, we needed access to deep UV photometry, good redshift estimates, and a measure of compactness and surface brightness. These three datasets are available in the COSMOS field (Scoville et al. 2007). We utilized the UV photometry from *GALEX* (Zamojski et al. 2007) and the HST (F814W) imaging (Koekemoer et al. 2007) to provide an accurate measure of the size and UV luminosity of the source, and the photometric redshift estimates of Mobasher et al. (2007). From these data, we select targets whose rest-frame UV luminosity, L_{FUV} , and surface brightness, I_{FUV} , are the same as those of LBGs.

We selected non-point sources with large L_{FUV} and

I_{FUV} analogous to LBGs (see Figure 1). From these we discard a small number (~ 15) which we find by visual inspection to have technical problems not obvious in the catalog, such as a close proximity to the edge of the *GALEX* field of view which suffers from artifacts. There are 32 sources remaining which meet our criteria. These sources are the brightest UV galaxies at $z \sim 0.7$, but their luminosity ($\log L_{UV} \gtrsim 10.4 L_\odot$) is similar to that of typical LBGs at $z \sim 3$. An $\sim L^*$ galaxy at $z > 6$ would fall at the faint end of the same range. The UV luminosity of the targets corresponds to a star formation rate (SFR) of $8\text{--}45 M_\odot/\text{yr}$, without correcting for dust extinction.

The 32 selected galaxies (see figure 2) share many observable properties with LBGs. By inference, they are the rare, young, strongly star-forming objects at moderate redshift that have just reached an evolutionary stage which was common at $z \sim 3$. A caveat to note regarding the sample selection is that the UV surface brightness our targets was derived using the sizes estimated from rest-frame optical ACS images, which are typically larger than the sizes measured by rest-frame UV images as in the case for the Hoopes et al. (2007) criteria.

3. OBSERVATIONS AND REDUCTIONS

3.1. Slitless UV Spectroscopy

The SBC uses a Multi-Anode Microchannel Array (MAMA) that has no read noise and is not sensitive to cosmic rays (Boffi 2007). Targets were positioned to land on the lower right quadrant of the detector to minimize the dark current “glow”, which was noted by Teplitz et al. (2006) to increase with exposure time.

The SBC field of view is $31'' \times 35''$, with a plate-scale of $0.032'' \text{ pixel}^{-1}$. The SBC PR130L, which covers 1250\AA to 2000\AA with a variable dispersion from $1.65\text{\AA} \text{ pixel}^{-1}$ at 1250\AA to $20.2\text{\AA} \text{ pixel}^{-1}$ at 1800\AA is used because it is not sensitive to the Ly α airglow which dominates the background in the PR110L prism. The PR130L prism is still sensitive to other airglow lines so the observations were taken with the SHADOW constraint reducing the airglow by a factor of 10.

The sources have a median *GALEX* near-UV magnitude of 22.5 (AB), and required 1–4 orbits in the shadow position (1500s/orbit; see Table 1 for details). Direct imaging (two 480s exposures/orbit) of our targets at 1600\AA was also acquired in the same visit with the F150LP filter to establish a zero-point of the wavelength scale. These data were taken over December 2007 – January 2009 in Cycle 16. An example of the direct SBC image and corresponding 2D spectra is shown in Figure 3 for a typical starburst galaxy in our sample and the target which is an AGN-starburst composite (see section 5.1 for a discussion).

The flat-fielding and dark subtraction of the SBC data was performed by the *HST* pipeline. Since this work relies on the measurement of flux below the Lyman limit, which is typically on the order of the sky background, sky subtraction must be done with care. The mean value for a region of sky, typically 300 pixels by 150 pixels above and below the target is measured for each prism exposure. The average sky background in each individual exposure is subtracted from each flat fielded prism image. The spectra were extracted in PyRAF using the *aXe*

slitless spectroscopy reduction package (ver. 1.6 Walsh et al. 2006; Kümmel et al. 2006), specifically designed for *HST* grism and prism data.

In the extraction, the position of the galaxy on the direct image is used in combination with the header dither parameters to locate the spectrum on the dispersed image and assigns a wavelength to each pixel in the spectrum. The spectral trace and wavelength solutions are defined with respect to a reference position, which is measured by running SExtractor (Bertin & Arnouts 1996) on a direct image for each orbit. A master catalog was generated for each set of prism images taken in a single orbit. Using the master catalogs the *aXe* software generates pixel extraction tables (PETs), which contain a spectral description for each pixel in the spectrum. Various sizes for the extraction window were explored, with an extraction width approximately the size of the object maximizing the signal to noise of the spectra. The signal to noise was further increased (a factor of 1.4) by using *aXe*'s optimal weighting extraction, which weights the pixels as a function of distance from the spectral trace rather than giving each pixel the same weight when generating the one dimensional spectra. The wavelength solution over 1300 to 1700Å is accurate to within a few angstroms. The spectra were flux calibrated using a known sensitivity curve for the PR130L prism (Larsen et al. 2006).

The flux and wavelength calibrated spectra for each prism image were co-added weighting each exposure by the rms of the background in each individual exposure. This was done to account for increasing dark current with subsequent exposures. For an individual target the dark current was a factor of four higher in the forth orbit compared to the first. The uncertainty in the spectral flux was estimated differently for the wavelengths regions red-ward and blue-ward of the Lyman limit. Blue-ward of 912Å where no signal is measured, and we are essentially probing the background. The standard deviation of the sky flux between the observed wavelengths typically used to measure the LyC in our $z \sim 0.7$ sample was found to be comparable to the standard deviation of the flux in the same wavelength region of the actual targets. We therefore use the standard deviation of the flux over 780-860Å rest-frame (the region used to measure LyC flux limits) as a conservative estimate of the uncertainty. Red-ward of the Lyman break, where flux is detected the errors at each wavelength bin in the final 1D co-added spectra are the 1σ weighted standard deviation. The final 1D spectra are presented in 7.

3.2. Optical Spectroscopy

Accurate spectroscopic redshifts are required to identify the observed wavelengths corresponding to the rest-frame Lyman limit and Lyman continuum. Redshifts cannot be measured from the FUV spectra themselves since the prism probes blue-ward of Ly- α in the rest-frame and the resolution is too poor. The photometric redshifts, although sufficient for selection purposes, have an uncertainty corresponding to $\sim 200\text{Å}$ at $z \sim 0.7$. Optical spectroscopy for 6 of our targets were taken from the public zCOSMOS program¹² (Lilly et al. 2009). An

additional 23 spectra were obtained at the Palomar Hale 5m Telescope using the Double Spectrograph (hereafter Double Spec; Oke & Gunn 1982) in February 2008 and 2009 with seeing conditions ranging from 1" to 2.5" for the majority of the observations and light cirrus. This instrument uses a pair of CCD cameras which simultaneously obtain long-slit spectra over a "blue" range of 3500Å to 5600Å and a "red" range of 6000Å to 8500Å. The observing strategy consisted of acquiring a series of 600-900s exposures with a slit width of 1.5". We obtained a total integration time of 40-90 mins for each of the 23 galaxies.

The data were reduced using standard IRAF tasks and wavelength calibrated with He, Ne, and Ar reference lamps. The spectral features used for the redshift determination were typically a combination of O[II] at 3727Å, O[III] at 5007Å and in some cases H β at 4861Å. The spectroscopic redshifts confirmed that all the galaxies were within the $0.6 < z < 0.85$ range needed to measure the escape fraction with the UV observations. The mean spectroscopic redshift of the sample is $z=0.679$. Due to poor observing conditions three targets remain with no spectroscopic redshift confirmation. Since only one of these (C-UVLG-15) had a detectable UV spectrum and the rest of the sample had photometric redshifts within a few percent of the spectroscopic redshift we assumed the photometric redshift for this galaxy.

4. DERIVING THE ESCAPE FRACTION

Typically, the escape fraction of Lyman Continuum photons is measured relative to the number of photons escaping at $\lambda_{rest} = 1500\text{Å}$ (Steidel et al. 2001). This allows a straightforward calculation of the escape fraction with only two flux measurements (at 1500Å and in the Lyman Continuum) using the following equation:

$$f_{esc,rel} = \frac{(f_{1500}/f_{LyC})_{int}}{(f_{1500}/f_{LyC})_{obs} \times (S)} \times \exp(\tau_{IGM,LyC}), \quad (1)$$

where $(f_{1500}/f_{LyC})_{int}$ and $(f_{1500}/f_{LyC})_{obs}$ are the intrinsic and observed Lyman continuum flux density ratios. The "LyC" refers to the wavelength at which Lyman continuum is measured (780-860Å for this study), S is the scaling factor discussed below and $\tau_{IGM,LyC}$ is the IGM optical depth for Lyman continuum photons along the line of sight to the galaxy. The intrinsic drop between the rest-frame FUV (1500Å) and the LyC (700-900Å) is highly uncertain and can not be observed. The assumed value of $(f_{1500}/f_{LyC})_{int}$ has varied by study from 3 (Steidel et al. 2001; Shapley et al. 2006) to 6 or 8 (Siana et al. 2007).

Since we probe LyC radiation at slightly bluer wavelengths at 830Å compared with (Steidel et al. 2001; Shapley et al. 2006) we used the SEDs of Bruzual & Charlot (2003) and estimated the break amplitude for f_{1500}/f_{830} to be 3.4 based on $f_{1500}/f_{900} = 3$. We assume a factor of ~ 1.2 reduction in f_{LyC}/f_{1500} for the neutral hydrogen opacity in the IGM, modeled in the same manner as Madau (1995) and Siana et al. (2007). The SBC spectra do not measure rest-frame 1500 Å for our targets. So, to calculate the escaping UV photons at 1500Å we use the flux within our spectrum between rest-frame 1000-1050Å and apply a scaling factor (S) to estimate the flux at 1500Å (f_{1500}). The sources in our sample are by

¹² Based on zCOSMOS observations carried out using the Very Large Telescope at the ESO Paranal Observatory under Programme ID: LP175.A-0839

selection, blue objects with low levels of extinction. Fits to the photometry suggest an $E(B - V) \sim 0.3$. Assuming 0.4 solar metallicity, constant star formation with a 300 Myr old population the scaling factor to go from the f_{1025} to f_{1500} is 1.5 in f_λ . The fluxes derived from the spectra are consistent with aperture photometry derived using the F150LP images.

Due to the slitless nature of the spectra there is spectral “smearing” along the dispersion direction proportional to the spatial size of the object. A different red wavelength cutoff was assumed for each object based on the galaxy’s size in the SBC direct image to ensure that light red-ward of the Lyman limit did not contaminate the LyC flux measurement. The sources have typical radii of $\sim 7\text{-}20$ pixels in F150LP corresponding to a red cutoff of range of $\sim 820\text{-}880\text{\AA}$. Furthermore, the sensitivity drops sharply at the blue end and therefore consider only the regions at rest wavelengths $> 780\text{\AA}$. The final spectral region used when estimating the LyC flux is between $\sim 780\text{-}880\text{\AA}$ with the red cutoff changing as a function of galaxy size (shaded regions in Figure 7).

The continuum is relatively flat around 850\AA for galaxies that are actively forming stars (Bruzual & Charlot 2003), like those in our sample. We therefore integrate the observed spectrum over several resolution elements to increase the signal-to-noise ratio. The wavelength solutions of the SBC, are accurate to a few angstroms between observed 1300\AA and 1700\AA over the SBC field-of-view, and the flux calibrations over this wavelength range are accurate to approximately 5% (Larsen 2006). The flux below the Lyman limit (f_{830}) is taken to be the average flux between $780\text{-}880\text{\AA}$ (again the red cutoff depends on the galaxy size). The uncertainty in f_{830} is derived using the following equation,

$$f_{er,830} = \frac{\sqrt{\sum(\Delta f_{er}^2 \times \Delta\lambda^2)}}{\Delta\lambda_{tot}}, \quad (2)$$

where Δf_{er} is the standard deviation of the flux over the assumed LyC region, $\Delta\lambda$ is the size of each pixel in angstroms (this value changes as a function of wavelength), and $\Delta\lambda_{tot}$ is the total wavelength range being averaged. The amount of escaping radiation below the Lyman limit is typically reported using a *relative* escape fraction (defined earlier in this section) or through a UV-to-Lyman continuum flux density ratio ($f_\nu(1500\text{\AA})/f_\nu(830\text{\AA})$). The former measure however, requires an assumption for the intrinsic Lyman break which is not well constrained. In the next section we present both the UV to Lyman continuum flux density ratios and the inferred relative escape fractions for completeness.

5. RESULTS

We find no direct detections of Far-UV flux in our sample of $32 z \sim 0.7$ LBG analogs. Nine galaxies (C-UVLG-3, 9, 10, 13, 14, 16, 22, 31, 32) were not detected in the direct F150LP image or PR130L spectra. The non-detections are likely due to in part to their large size which resulted in UV surface brightnesses below the sensitivity of our observations. Another likely contributing factor is that 7/9 of the undetected galaxies had the largest extinctions within our sample $\gtrsim 0.3$.

The observed flux density ratio, $f_\nu(1500)/f_\nu(830)$, in the individual sources range from 20 to 204 with a median

of 73.5 (3σ lower limits). In order to convert these ratios into a *relative* escape fraction we apply equation (1) assuming an IGM transmission of 0.85 and a value of 3.4 or 7 for the intrinsic Lyman break (see Table 1). Our far-UV sensitivities give $f_{esc,rel}$ close to zero, with individual 3σ upper limits ranging from 0.01 – 0.19. To increase our sensitivity further, we stacked the non-detections with UV sizes $\lesssim 0''.78$ in diameter, which corresponds to a red cutoff of $\sim 860\text{\AA}$. This red cutoff was chosen to maximizing the number of galaxies in the stack while probing as closely to the Lyman limit as possible. The stack was composed of 18 galaxies placing an upper limit on $f_\nu(1500)/f_\nu(830)$ of 378.7 and a $f_{esc,rel} < 0.01$ (see Figure 6). In addition to the global stack we separated the sample by morphology, stacking the 8 galaxies which appeared in the *HST* F814W filter to be undergoing a merger event and a radius of $\leq 0''.7$ (red cut off of 865\AA). We find 3σ upper limits for $f_\nu(1500)/f_\nu(830)$ of 223.2 and a $f_{esc,rel} < 0.02$ for galaxy mergers (see Figure 7 and section 6.3 for further discussion).

5.1. LyC Emission: AGN and Star Formation?

Flux below the Lyman limit was detected in C-UVLG-17 (hereafter T17), however it is unclear what process is responsible for the FUV emission (see Figure 4). T17 is detected in the X-ray with a luminosity of $\sim 2 \times 10^{43} \text{ ergs sec}^{-1}$ (2-10KeV), and is a Type 2 AGN based on the optical spectrum. Although it is highly probable that the LyC flux is coming from the AGN it is possible that some flux has its origin in young massive star formation. The COSMOS 30 photometric band ($0.14\text{-}8\mu\text{m}$) best-fit SED is a pure starburst, the IRAC colours do not place T17 in the locus of optically bright unobscured AGN and is non-variable (over a five year period). The spectrum shows no break at the Lyman limit, with ionizing flux detected down to $\lambda \sim 810 \text{ \AA}$. Below this wavelength, the continuum is strongly suppressed, indicative of a foreground, high column density absorber at $z \sim 0.55$. This source is interesting as an example of leaking LyC from a composite AGN star forming galaxy.

5.2. Foreground Contamination

Higher redshift ($z \sim 3$) studies have detected LyC photons in approximately 10% of galaxies (Shapley et al. 2006; Iwata et al. 2009). Vanzella et al. (2010) estimate the at ~ 3 there is a 50% probability that 1/3 of the galaxies with *directly* detected LyC emission are the result of foreground contamination by low redshift blue galaxies within $\sim 1''$ of the high redshift galaxy. Figure 9 highlights an example of foreground contamination found in our sample. The NUV *GALEX* magnitude which is used in our sample selection has a PSF of $\sim 4''$ which encompasses both galaxies.

The high resolution *HST* F814W image (Scoville et al. 2007) reveals two galaxies separated by $\sim 1.2'' (< 10\text{kpc})$, exhibiting irregular morphologies consistent with a close galaxy pair. The southern galaxy (hereafter GalA) has two compact nuclei and evidence of long tidal tails. The northern galaxy (hereafter GalB) exhibits multiple star formation knots, an asymmetric morphology and tidal tails. The two primary UV bright knots that make up GalB are referred to as GalB1 and GalB2 as noted in Figure 9.

Although GalA was the intended target in our program the high resolution SBC direct F150LP image revealed that GalB dominated the NUV and FUV flux. The *Spitzer* 24 μm detection is centered on GalA corresponding to an IR luminosity of $L_{[8-1000\mu\text{m}]} = 2.3 \times 10^{11} L_\odot$ and a SFR of $\sim 40 M_\odot/\text{yr}$ (Kennicutt 1998). GalA was not detected in the FUV (likely due to its high dust content), however the UV spectrum of GalB2 (Figure 10) would imply a *relative* escape fraction, $f_{rel,esc}$ of $30\% \pm 6\%$ and a $f_\nu(1500\text{\AA})/f_\nu(830\text{\AA}) = 14.3$, if it was at the same redshift as GalA. Follow-up spectra with Keck DEIMOS revealed that GalB was in fact a low redshift interloper at $z=0.19$. The close ($\sim 1''$) projected separation of these galaxies is a good example of foreground contamination and could explain some the $z \sim 3$ detections of Iwata et al. (2009) particularly the ones with a $\sim 1''$ offset between the LyC emission and assumed LBG counterpart.

6. DISCUSSION

The deep UV spectra presented here achieve the lowest individual limits of the ionizing escape fraction at any redshift. We confirm the results of shallower studies that suggest low escape fractions in moderate redshift starbursts. We now present our findings in the context of recent studies and discuss some possible mechanisms that could be responsible for the apparent lack of $z \sim 1$ starbursts with large escape fractions.

6.1. Comparison with Recent Work

Recently, Siana et al. (2010) used HST ACS/SBC 1500 \AA imaging and obtain a stacked 3σ limit of $f_\nu(700)/f_\nu(1500) < 0.02$. With the inclusion of previous studies (Malkan et al. 2003; Siana et al. 2007) they state that no more than 8% of star-forming galaxies at $z \sim 1$ have relative escape fractions greater than 0.50. Cowie et al. (2008) stacked the GALEX far-UV (1500 \AA) fluxes of a much larger sample (626 galaxies) and obtain a similar 3σ upper limit of $f_\nu(700)/f_\nu(1500) < 0.012$, confirming that starbursts at $z \sim 1$ have low ionizing emissivities. All of these studies have used broad-band UV imaging to probe the Lyman continuum at $\sim 700\text{\AA}$ whereas the detections at $z \sim 3$ have been obtained through spectroscopy (Steidel et al. 2001; Shapley et al. 2006) and narrow-band imaging (Iwata et al. 2008) where the Lyman continuum is sampled just below the Lyman limit (880 – 910 \AA).

This is the first $z \sim 1$ spectroscopic study to provide Lyman continuum measurements much closer to the Lyman limit and is therefore more directly comparable to these higher redshift studies. Shapley et al. (2006), with a sample of 14 LBGs probe a slightly higher UV luminosity and detect two objects with large escape fractions (with LyC-to-UV ratios significantly above our limits). One of these objects likely has a lower escape fraction than initially reported as it was not detected in deep narrow-band imaging probing the Lyman continuum (Iwata et al. 2009). Therefore, only one of 14 objects has a significant detection. Similarly, Iwata et al. (2009), which probe comparable rest-frame UV luminosities as our $z < 1$ sample, detect large escape fractions in $\sim 10\%$ of LBGs and Ly α emitters at $z = 3.1$. If the LBG analogs in our sample have ionizing properties similar to

LBGs at $z \sim 3$, we would expect to detect ~ 3 objects with large fractions of escaping LyC radiation, however we detect zero. Our individual limits are significantly better than the studies at $z = 3$, so if there are significant numbers of galaxies with lower escape fractions (e.g. $f_{esc,rel} \sim 0.20$, rather than unity), we would be able to detect them. We see no evidence for this scenario in our sample. Comparing our findings, which are in agreement with all other $z < 1$ f_{esc} measurements, with $z \sim 3$ studies (Shapley et al. 2006; Iwata et al. 2009) implies that the average escape fraction evolves with redshift, but the cause of this evolution remains unknown. We proceed by exploring possible mechanisms to explanation that lack of large escape fraction galaxies at $z \sim 1$.

6.2. Selecting Analogs of High f_{esc} LBGs

When comparing high and low redshift galaxy samples there is always some degree of uncertainty regarding the true analog nature of the two populations. As discussed in section 2 and shown in Figure 1 we selected a sample of LBG analogs sharing many of the same properties as the $z \sim 3$ LBGs observed by Shapley et al. (2006) and Iwata et al. (2009). Figure 8, further highlights their similarities showing the distribution of reddening, stellar mass and rest-frame UV luminosity in these sources is similar to the distribution in LBGs. The similarity in mass together with the UV-optical colors of the UVLGs imply that they may still be undergoing an early, major episode of star formation, rather than a small burst on top of a hidden older population (also see Barmby et al. 2004, for the same reason applied to LBGs).

Ultimately, this sample of LBG analogs shares numerous similarities to the parent LBG population, but since only $\sim 10 - 15\%$ of LBGs have been observed with significant LyC detections, perhaps this subclass of LBGs have other processes at work allowing or aiding in the escape of LyC photons.

6.3. Galaxy Mergers

Galaxy mergers offer an intriguing explanation for the increased escape fraction seen at $z \sim 3$. Overzier et al. (2008) noted that UVLG typically exhibit faint tidal features suggestive of a merger or recent interaction. They therefore propose that the super starbursts in LBGs are triggered by gas-rich mergers. As galaxies collide, strong gravitational and tidal forces can expel long streams of stars, and ignite violent starbursts at rates of a few to hundreds of M_\odot/yr (Schweizer 1982; Barton et al. 2000; Bridge et al. 2010). During a merger, the tidal fields distort the galaxies radially, drawing out galactic material into long tails, plumes and bridges (e.g. Toomre & Toomre 1972; Mihos & Hernquist 1996). The HI reservoirs can become disturbed, and the neutral gas pulled away from the sources of ionizing radiation producing low-column density lines of sight (Hibbard et al. 2000; de Mello et al. 2008) through the galaxies, in turn allowing the escape of LyC photons. Simulations by Gnedin et al. (2008) suggest that the escape fraction in major mergers can be large ($f_{esc,rel} \gtrsim 30\%$) compared to non-mergers ($f_{esc,rel} < 10\%$) along specific lines of sight. Within our sample of 32 galaxies, 11 had morphologies consistent with merger activity. We independently stacked 8 of these spectra (removing 3 due to their larger spatial extent) and find $f_{esc} < 2\%$ (3σ upper limit).

If merging is a viable mechanism for clearing pathways in the ISM for LyC photons, the orientation of the system along the line of sight is also a likely factor, requiring a large sample of UV luminous mergers. Therefore, we cannot say whether mergers are an important factor as our sample size is at present too small. Currently, there is a lack of deep high resolution rest-frame optical imaging of the LBGs with larger escape fractions, and the interpretation of UV morphologies remains problematic (Law et al. 2007). Future near-IR observations with *HST* of the $z \sim 3$ LGB leakers will shred light on this hypothesis.

As discussed earlier in the section, galaxy mergers are capable of clearing pathways, exposing UV bright stars. If mergers do facilitate the escape of LyC radiation then an evolving merger rate, may be responsible for the observed evolution in f_{esc} . Numerous observational studies and simulations haven shown that the galaxy merger rate evolves with redshift, going as $\sim (1+z)^{2-3}$ (Gottlöber et al. 2001; Conselice et al. 2003; Kartaltepe et al. 2007; Hopkins et al. 2007; Bridge et al. 2007; Conselice et al. 2008; Bridge et al. 2010). The factor of 3-4 increase in merger rate between $z \sim 1 - 3$ as seen observationally, would also increase the the number of lines-of-sights and range of encounter parameters observed in $z \sim 3$ galaxy mergers by the same factor. This would in turn increase the likelihood of detecting LyC at higher redshift.

6.4. Evolving f_{esc} : Size, Mass, & Star Formation

The LyC escape fraction is limited by the distribution of neutral hydrogen along a line-of-sight and likely depends on galactic parameters. We now consider what galaxy properties could evolve with redshift that reduce the efficiency of galactic outflows/chimneys in leaking LyC photons from luminous galaxies.

Typical galaxies (including UV bright galaxies) have been shown to be 1.5 to 3 times smaller at $z \sim 3$ than there local counterparts (Trujillo et al. 2006; Papovich & Bell 2002; Ferguson et al. 2004). Although our LBG analog sample was selected to have similar UV surface brightnesses as $z \sim 3$ LBGs (refer to Figure 1), little is known about the true optical sizes of LBGs or the distribution of gas. The velocities of galactic winds or outflows have been found to be proportional to the SFR in LBGs (Ferrara & Ricotti 2006), therefore LBG and LBG analogs, having similar SFR should in principle generate outflows with similar velocities (a few hundred km s^{-1}). However, smaller galaxies would have higher SFRs per unit volume, which can result in more efficient galactic winds (Veilleux et al. 2005), more easily clearing pathways or “chimney-like” structures, and in turn allowing for higher f_{esc} (Fujita et al. 2003).

With smaller galaxies, and higher-density starbursts comes the potential for a larger fraction of stars born in very compact star clusters, including super star clusters (SSCs). SSCs can have thousands of young ($< 50\text{Myr}$) stars within a half-light radius of $\sim 10\text{pc}$ (Veilleux et al. 2005). These extreme concentrations of hot O and B stars can greatly impact the state of the ISM driving powerful galactic winds (like those seen in M82), opening channels for the escaping LyC photons. SSCs have been detected in the tidal tails (Charlton et al. 2009) and outer regions of galaxies, which could explain the spatially offset LyC emission (to the optical emission) detected by Iwata et al. (2009) in a few $z \sim 3$ LBGs.

There is also some evidence that SSCs found in the local group of galaxies have top-heavy IMFs (Harayama et al. 2008), which enhance the efficiency in clearing lines-of-sight, due to the larger outflow velocities generated by massive stars.

Another property which has been shown to possibly evolve with redshift is the stellar mass-to-dark matter ratio. Recent work by Epinat et al. (2009) and Lethaud & Capak (2009), have reported that local massive galaxies have more centrally concentrated dark matter than higher redshift galaxies ($z \sim 0.7$) with comparable stellar masses. A higher stellar mass-to-dark matter mass ratio at lower redshift would result in a larger gravitational potential, and in turn the requirement for larger galactic winds to achieve the same “porosity” of the ISM (and the probability for ionizing photons to escape their host galaxies). Thicker disks due to dense concentrations of gas have also been shown in to impede or slow the development of galactic outflows, due to a higher gravitational potential (Cooper et al. 2008).

6.5. Intrinsic LyC-to-UV Ratio: A Top-Heavy IMF?

An evolving intrinsic LyC-to-UV flux density ratio could also be responsible for the observed evolution in f_{esc} . The escape fraction is measured by comparing the UV (1500Å) flux of a galaxy to flux below the Lyman limit. One key assumption that is made involves the inherent LyC-to-UV ratio of starbursts. Typically, this ratio is considered constant with redshift, but if there were an order of magnitude larger production rate of the LyC relative to the 1500Å, flux at $z > 3$ than at $z < 1$, the observed change in f_{esc} would be expected.

Iwata et al. (2009) noted that ~ 3 LBGs in their sample had spectral energy distributions intrinsically bluer than those expected from population synthesis models, assuming a standard IMF with moderate dust attenuation. They show that an intrinsically bluer spectral energy distribution (~ 0.3 mags bluer in NB359-R than those of Starburst99), in the absence of QSO activity, can be produced with a top-heavy initial mass function (IMF). They also suggest that a deviation from the Calzetti et al. (2000) dust attenuation law, with less dust absorption at 900Å, compared to that at 1500Å, can come close to achieving the observed bluer colors of those LBGs.

It has been shown that the UV luminosity density at $z \sim 6$ may be insufficient to explain the ionized Universe at $z > 7$ unless the IMF allowed for the production of more massive stars (Chary 2008). A top-heavy IMF at higher redshift could help explain the larger number of LyC detections at $z \sim 3$ as massive stars produce more LyC photons, and stronger supernova driven winds. A top-heavy IMF requires regions of potentially low metallicity gas which is consistent with the metallicity and dust evolution seen from $z \sim 3$ to 1 Ferguson et al. (2002).

7. SUMMARY

Lyman continuum photons produced in massive starbursts likely played an important role in the reionization of the Universe. However, their contribution depends upon the fraction of ionizing radiation that can escape the high column density of HI gas surrounding these star-forming galaxies. We have presented HST rest-frame UV slitless spectroscopy of 32 $z \sim 0.7$ LBG analogs in the

COSMOS field to investigate the LyC escape fraction. These UV spectra have achieved the deepest limits to date on the escape fraction in individual sources at any redshift. A summary of our results are as follows.

We find no direct detections of LyC, consistent with other low redshift studies. The individual 3σ upper limits of $f_{\nu}(1500\text{\AA})/f_{\nu}(830\text{\AA})$ ratio range from 20 to 204 (median of 73.5) and 378.7 in the stack of 18 galaxies. Assuming an intrinsic Lyman break of 3.4 and an optical depth of 85% we report a *relative* escape fraction in individual galaxies of 0.02–0.19 and 0.01 in the stack (3σ upper limit). There is no indication of the near unity escape fractions found at $z \sim 3$. The striking contrast between the nearly zero escape fractions found in all 32 $z \sim 0.7$ LBG analogs with the near unity escape fractions discovered in 10% of the $z \sim 3$ LBG population strongly argues for an evolving escape fraction. It is unclear however if the lack of near unity escape fraction detections at low redshift is due to an evolution in f_{esc} itself, or that the number of galaxies with large amounts of leaking LyC evolves with redshift. Possible causes for a change in the escape fraction with redshift involve a top-heavy IMF, larger SFR densities, stellar mass-to-dark matter ratios, and/or fraction of SSCs at higher redshifts. All these mechanisms enhance the efficiency of galaxy winds, increasing the porosity of the ISM, facilitating LyC escape. However, if galaxy mergers aid in the escape of LyC radiation then an evolving galaxy merger rate could account for the high number of LyC leaking

galaxies at $z \sim 3$. The lack of low redshift galaxies with escaping LyC could then be explained by the small number of galaxy mergers that have been observed below the Lyman limit.

The escape fraction of UV radiation in $z \sim 1$ luminous starburst galaxies is an important quantity to understand since it provides insight into the sources (massive star formation or QSOs) responsible for reionization. Our study has presented a robust measure of the f_{esc} in the low redshift Universe and suggests that the escape fraction in objects that are analogous to the galaxies thought responsible for reionization evolves with redshift. However future study is required to isolate the cause of this evolution.

The research described in this paper was carried out, in part, by the Jet Propulsion Laboratory, California Institute of Technology, and observations obtained at the Hale Telescope, Palomar Observatory as part of a continuing collaboration between the California Institute of Technology, NASA /JPL, and Cornell University. This work was sponsored by the National Aeronautics and Space Administration (NASA). Support for programs XXX and XXX was provided by NASA through grants from the Space Telescope Science Institute, which is operated by the Association of Universities for Research in Astronomy, Inc., under NASA contract NAS 5-26555.

REFERENCES

- Barmby, P., Huang, J.-S., Fazio, G. G., Surace, J. A., Arendt, R. G., Hora, J. L., Pahre, M. A., Adelberger, K. L., Eisenhardt, P., Erb, D. K., Pettini, M., Reach, W. T., Reddy, N. A., Shapley, A. E., Steidel, C. C., Stern, D., Wang, Z., & Willner, S. P. 2004, ApJS, 154, 97
- Barton, E. J., Geller, M. J., & Kenyon, S. J. 2000, ApJ, 530, 660
- Bertin, E., & Arnouts, S. 1996, A&AS, 117, 393
- Boffy, F. 2007, ApJ
- Bouwens, R. J., Illingworth, G. D., Blakeslee, J. P., & Franx, M. 2006, ApJ, 653, 53
- Bridge, C. R., Appleton, P. N., Conselice, C. J., Choi, P. I., Armus, L., Fadda, D., Laine, S., Marleau, F. R., Carlberg, R. G., Helou, G., & Yan, L. 2007, ApJ, 659, 931
- Bridge, C. R., Carlberg, R. G., & Sullivan, M. 2010, ApJ, 709, 1067
- Bruzual, G., & Charlot, S. 2003, MNRAS, 344, 1000
- Calzetti, D., Armus, L., Bohlin, R. C., Kinney, A. L., Koornneef, J., & Storchi-Bergmann, T. 2000, ApJ, 533, 682
- Charlton, J. C., Mullan, B., Lee, K., Knierman, K., Gronwall, C., Gallagher, S., Maybhate, A., Durrell, P., Hibbard, J., Bastian, N., Vacca, W., Palma, C., & Hunsberger, S. 2009, in American Astronomical Society Meeting Abstracts, Vol. 213, American Astronomical Society Meeting Abstracts, 344.01
- Chary, R.-R. 2008, ApJ, 680, 32
- Conselice, C. J., Bershady, M. A., Dickinson, M., & Papovich, C. 2003, AJ, 126, 1183
- Conselice, C. J., Rajgor, S., & Myers, R. 2008, MNRAS, 386, 909
- Cooper, J. L., Bicknell, G. V., Sutherland, R. S., & Bland-Hawthorn, J. 2008, ApJ, 674, 157
- Cowie, L. L., Barger, A. J., & Trouille, L. 2008, ArXiv e-prints
- de Mello, D. F., Smith, L. J., Sabbi, E., Gallagher, J. S., Mountain, M., & Harbeck, D. R. 2008, AJ, 135, 548
- Deharveng, J.-M., Buat, V., Le Brun, V., Milliard, B., Kunth, D., Shull, J. M., & Gry, C. 2001, A&A, 375, 805
- Epinat, B., Contini, T., Le Fevre, O., Vergani, D., Amram, P., Garilli, B., Queyrel, J., Tasca, L., & Tresse, L. 2009, ArXiv e-prints
- Ferguson, H. C., Dickinson, M., Giavalisco, M., Kretchmer, C., Ravindranath, S., Idzi, R., Taylor, E., Conselice, C. J., Fall, S. M., Gardner, J. P., Livio, M., Madau, P., Moustakas, L. A., Papovich, C. M., Somerville, R. S., Spinrad, H., & Stern, D. 2004, ApJ, 600, L107
- Ferguson, H. C., Dickinson, M., & Papovich, C. 2002, ApJ, 569, L65
- Ferrara, A., & Ricotti, M. 2006, MNRAS, 373, 571
- Fujita, A., Martin, C. L., Mac Low, M.-M., & Abel, T. 2003, ApJ, 599, 50
- Giallongo, E., Fontana, A., & Madau, P. 1997, MNRAS, 289, 629
- Gnedin, N. Y., Kravtsov, A. V., & Chen, H.-W. 2008, ApJ, 672, 765
- Gottlöber, S., Klypin, A., & Kravtsov, A. V. 2001, ApJ, 546, 223
- Harayama, Y., Eisenhauer, F., & Martins, F. 2008, ApJ, 675, 1319
- Heckman, T. M., Hoopes, C. G., Seibert, M., Martin, D. C., Salim, S., Rich, R. M., Kauffmann, G., Charlot, S., Barlow, T. A., Bianchi, L., Byun, Y.-I., Donas, J., Forster, K., Friedman, P. G., Jelinsky, P. N., Lee, Y.-W., Madore, B. F., Malina, R. F., Milliard, B., Morrissey, P. F., Neff, S. G., Schiminovich, D., Siegmund, O. H. W., Small, T., Szalay, A. S., Welsh, B. Y., & Wyder, T. K. 2005, ApJ, 619, L35
- Hibbard, J. E., Vacca, W. D., & Yun, M. S. 2000, AJ, 119, 1130
- Hoopes, C. G., Heckman, T. M., Salim, S., Seibert, M., Tremonti, C. A., Schiminovich, D., Rich, R. M., Martin, D. C., Charlot, S., Kauffmann, G., Forster, K., Friedman, P. G., Morrissey, P., Neff, S. G., Small, T., Wyder, T. K., Bianchi, L., Donas, J., Lee, Y.-W., Madore, B. F., Milliard, B., Szalay, A. S., Welsh, B. Y., & Yi, S. K. 2007, ApJS, 173, 441
- Hopkins, P. F., Bundy, K., Hernquist, L., & Ellis, R. S. 2007, ApJ, 659, 976
- Inoue, A. K., Iwata, I., & Deharveng, J.-M. 2006, MNRAS, 371, L1
- Iwata, I., Inoue, A. K., Matsuda, Y., Furusawa, H., Hayashino, T., Kousai, K., Akiyama, M., Yamada, T., Burgarella, D., & Deharveng, J. 2008, ArXiv e-prints
- Iwata, I., Inoue, A. K., Matsuda, Y., Furusawa, H., Hayashino, T., Kousai, K., Akiyama, M., Yamada, T., Burgarella, D., & Deharveng, J.-M. 2009, ApJ, 692, 1287

- Jiang, L., Fan, X., Annis, J., Becker, R. H., White, R. L., Chiu, K., Lin, H., Lupton, R. H., Richards, G. T., Strauss, M. A., Jester, S., & Schneider, D. P. 2008, AJ, 135, 1057
- Kartaltepe, J. S., Sanders, D. B., Scoville, N. Z., Calzetti, D., Capak, P., Koekemoer, A., Mobasher, B., Murayama, T., Salvato, M., Sasaki, S. S., & Taniguchi, Y. 2007, ApJS, 172, 320
- Kennicutt, Jr., R. C. 1998, ARA&A, 36, 189
- Koekemoer, A. M., Aussel, H., Calzetti, D., Capak, P., Giavalisco, M., Kneib, J.-P., Leauthaud, A., Le Fèvre, O., McCracken, H. J., Massey, R., Mobasher, B., Rhodes, J., Scoville, N., & Shopbell, P. L. 2007, ApJS, 172, 196
- Kümmel, M., Larsen, S. S., & Walsh, J. R. 2006, in The 2005 HST Calibration Workshop: Hubble After the Transition to Two-Gyro Mode, ed. A. M. Koekemoer, P. Goudfrooij, & L. L. Dressel, 85+
- Larsen, S. S. 2006, Wavelength and Flux calibration of the ACS/SBC PR110L and PR130L prisms, Tech. rep.
- Larsen, S. S., Walsh, J., & Kümmel, M. 2006, Wavelength and Flux Calibration of the ACS/HRC PR200L Prism, Tech. rep.
- Law, D. R., Steidel, C. C., Erb, D. K., Pettini, M., Reddy, N. A., Shapley, A. E., Adelberger, K. L., & Simenc, D. J. 2007, ApJ, 656, 1
- Leitherer, C., Ferguson, H. C., Heckman, T. M., & Lowenthal, J. D. 1995, ApJ, 454, L19+
- Lethaud, A., & Capak, P. 2009, ApJ
- Lilly, S. J., Le Brun, V., Maier, C., Mainieri, V., Mignoli, M., Scudeggio, M., Zamorani, G., Carollo, M., Contini, T., Kneib, J., Le Fèvre, O., Renzini, A., Bardelli, S., Bolzonella, M., Bongiorno, A., Caputi, K., Coppa, G., Cucciati, O., de la Torre, S., de Ravel, L., Franzetti, P., Garilli, B., Iovino, A., Kampczyk, P., Kovac, K., Knobel, C., Lamareille, F., Le Borgne, J., Pello, R., Peng, Y., Pérez-Montero, E., Ricciardelli, E., Silverman, J. D., Tanaka, M., Tasca, L., Tresse, L., Vergani, D., Zucca, E., Ilbert, O., Salvato, M., Oesch, P., Abbas, U., Bottini, D., Capak, P., Cappi, A., Cassata, P., Cimatti, A., Elvis, M., Fumana, M., Guzzo, L., Hasinger, G., Koekemoer, A., Leauthaud, A., Maccagni, D., Marinoni, C., McCracken, H., Memeo, P., Meneux, B., Porciani, C., Pozzetti, L., Sanders, D., Scaramella, R., Scarlata, C., Scoville, N., Shopbell, P., & Taniguchi, Y. 2009, ApJS, 184, 218
- Madau, P. 1995, ApJ, 441, 18
- Madau, P., Haardt, F., & Rees, M. J. 1999, ApJ, 514, 648
- Malkan, M., Webb, W., & Konopacky, Q. 2003, ApJ, 598, 878
- Mihos, J. C., & Hernquist, L. 1996, ApJ, 464, 641
- Mobasher, B., Capak, P., Scoville, N. Z., Dahlen, T., Salvato, M., Aussel, H., Thompson, D. J., Feldmann, R., Tasca, L., Lefevre, O., Lilly, S., Carollo, C. M., Kartaltepe, J. S., McCracken, H., Mould, J., Renzini, A., Sanders, D. B., Shopbell, P. L., Taniguchi, Y., Ajiki, M., Shioya, Y., Contini, T., Giavalisco, M., Ilbert, O., Iovino, A., Le Brun, V., Mainieri, V., Mignoli, M., & Scudeggio, M. 2007, ApJS, 172, 117
- Oke, J. B., & Gunn, J. E. 1982, PASP, 94, 586
- Overzier, R. A., Heckman, T. M., Kauffmann, G., Seibert, M., Rich, R. M., Basu-Zych, A., Lotz, J., Aloisi, A., Charlot, S., Hoopes, C., Martin, D. C., Schiminovich, D., & Madore, B. 2008, ApJ, 677, 37
- Papovich, C., & Bell, E. F. 2002, ApJ, 579, L1
- Schweizer, F. 1982, ApJ, 252, 455
- Scoville, N., Abraham, R. G., Aussel, H., Barnes, J. E., Benson, A., Blain, A. W., Calzetti, D., Comastri, A., Capak, P., Carilli, C., Carlstrom, J. E., Carollo, C. M., Colbert, J., Daddi, E., Ellis, R. S., Elvis, M., Ewald, S. P., Fall, M., Franceschini, A., Giavalisco, M., Green, W., Griffiths, R. E., Guzzo, L., Hasinger, G., Impey, C., Kneib, J.-P., Koda, J., Koekemoer, A., Lefevre, O., Lilly, S., Liu, C. T., McCracken, H. J., Massey, R., Mellier, Y., Miyazaki, S., Mobasher, B., Mould, J., Norman, C., Refregier, A., Renzini, A., Rhodes, J., Rich, M., Sanders, D. B., Schiminovich, D., Schinnerer, E., Scudeggio, M., Sheth, K., Shopbell, P. L., Taniguchi, Y., Tyson, N. D., Urry, C. M., Van Waerbeke, L., Vettolani, P., White, S. D. M., & Yan, L. 2007, ApJS, 172, 38
- Shapley, A. E., Steidel, C. C., Erb, D. K., Reddy, N. A., Adelberger, K. L., Pettini, M., Barmby, P., & Huang, J. 2005, ApJ, 626, 698
- Shapley, A. E., Steidel, C. C., Pettini, M., Adelberger, K. L., & Erb, D. K. 2006, ApJ, 651, 688
- Siana, B., Polletta, M. d. C., Smith, H. E., Lonsdale, C. J., Gonzalez-Solares, E., Farrah, D., Babbedge, T. S. R., Rowan-Robinson, M., Surace, J., Shupe, D., Fang, F., Franceschini, A., & Oliver, S. 2008, ApJ, 675, 49
- Siana, B., Teplitz, H. I., Colbert, J., Ferguson, H. C., Dickinson, M., Brown, T. M., Conselice, C. J., de Mello, D. F., Gardner, J. P., Giavalisco, M., & Menanteau, F. 2007, ApJ, 668, 62
- Siana, B., Teplitz, H. I., Ferguson, H. C., Brown, T. M., Giavalisco, M., Dickinson, M., Chary, R., de Mello, D. F., Conselice, C. J., Bridge, C. R., Gardner, J. P., Colbert, J. W., & Scarlata, C. 2010, ArXiv e-prints
- Steidel, C. C., Pettini, M., & Adelberger, K. L. 2001, ApJ, 546, 665
- Teplitz, H. I., Siana, B., Brown, T. M., Chary, R., Colbert, J. W., Conselice, C. J., de Mello, D. F., Dickinson, M., Ferguson, H. C., Gardner, J. P., & Menanteau, F. 2006, AJ, 132, 853
- Toomre, A., & Toomre, J. 1972, ApJ, 178, 623
- Trujillo, I., Förster Schreiber, N. M., Rudnick, G., Barden, M., Franx, M., Rix, H.-W., Caldwell, J. A. R., McIntosh, D. H., Toft, S., Häussler, B., Zirm, A., van Dokkum, P. G., Labbé, I., Moorwood, A., Röttgering, H., van der Wel, A., van der Werf, P., & van Starkenburg, L. 2006, ApJ, 650, 18
- Vanzella, E., Siana, B., Cristiani, S., & Nonino, M. 2010, ArXiv e-prints
- Veilleux, S., Cecil, G., & Bland-Hawthorn, J. 2005, ARA&A, 43, 769
- Verma, A., Lehnert, M. D., Förster Schreiber, N. M., Bremer, M. N., & Douglas, L. 2007, MNRAS, 377, 1024
- Walsh, J. R., Kümmel, M., & Larsen, S. S. 2006, in The 2005 HST Calibration Workshop: Hubble After the Transition to Two-Gyro Mode, ed. A. M. Koekemoer, P. Goudfrooij, & L. L. Dressel, 79+
- Yan, H., Dickinson, M., Giavalisco, M., Stern, D., Eisenhardt, P. R. M., & Ferguson, H. C. 2006, ApJ, 651, 24
- Zamojski, M. A., Schiminovich, D., Rich, R. M., Mobasher, B., Koekemoer, A. M., Capak, P., Taniguchi, Y., Sasaki, S. S., McCracken, H. J., Mellier, Y., Bertin, E., Aussel, H., Sanders, D. B., Le Fèvre, O., Ilbert, O., Salvato, M., Thompson, D. J., Kartaltepe, J. S., Scoville, N., Barlow, T. A., Förster, K., Friedman, P. G., Martin, D. C., Morrissey, P., Neff, S. G., Seibert, M., Small, T., Wyder, T. K., Bianchi, L., Donas, J., Heckman, T. M., Lee, Y.-W., Madore, B. F., Milliard, B., Szalay, A. S., Welsh, B. Y., & Yi, S. K. 2007, ApJS, 172, 468

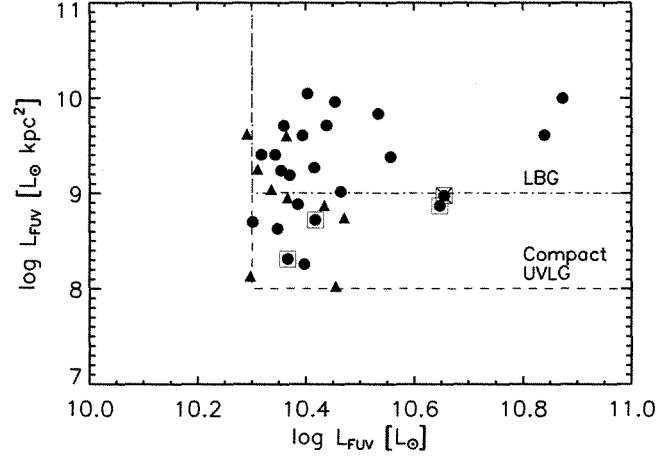


FIG. 1.— The FUV luminosity vs. FUV surface brightness for our sample of 32 galaxies (circles and triangles) with $0.65 < z < 0.85$ in COSMOS. The dash-dotted line indicates the region occupied by $z \sim 3$ LBGs, while the dashed line marks the region occupied by local compact UV luminous galaxies, thought to be analogs for $z \sim 3$ LBGs (Hoopes et al. 2007). The triangles highlight the galaxies that were not detected in the SBC prism observations. The open squares indicate galaxies with no ACS imaging, and the 'x' notes the target found to be an AGN-starburst composite (C-UVLG-17). Note that the angular sizes of our galaxies are derived using rest-frame optical ACS images, which are typically larger than the sizes measured by rest-frame UV images as in the case for the Hoopes et al. (2007).

TABLE 1
SBC OBSERVATIONS OF LBG ANALOGS IN THE COSMOS FIELD

Object ID	R.A. (J2000.0)	Decl. (J2000.0)	Exp. Time (mins)	z_{spec}	NUV ^a	$f_{\nu}830^b$	$(f_{\nu}1500/f_{\nu}830)_{obs}$	$f_{esc,rel}^c$	$f_{esc,rel}^d$
C-UVLG-02	149.94569	2.50422	108	0.667	22.40	2.880e-19	36.90	<0.108	<0.223
C-UVLG-05	150.08705	2.30905	108	0.688	22.60	1.708e-17	118.94	<0.034	<0.069
C-UVLG-07	150.21405	2.36754	108	0.669	22.69	9.144e-16	73.45	<0.054	<0.112
C-UVLG-08	150.42432	2.03343	81	0.685	22.35	7.305e-20	144.16	<0.028	<0.057
C-UVLG-11	150.15372	1.84970	108	0.670	22.39	6.471e-17	112.37	<0.036	<0.073
C-UVLG-12	149.85553	2.55685	108	0.665	22.50	1.054e-16	20.69	<0.193	<0.397
C-UVLG-15	150.27368	2.55358	108	0.715	22.60	3.243e-21	40.49	<0.099	<0.203
C-UVLG-18	150.60126	2.71238	108	0.676	22.53	1.671e-16	34.02	<0.118	<0.242
C-UVLG-19	150.48743	2.15107	108	0.684	22.41	4.484e-20	34.73	<0.115	<0.237
C-UVLG-20	150.51077	2.75674	81	0.675	22.09	5.094e-19	9312	<0.043	<0.088
C-UVLG-21	149.62891	2.19084	108	0.701	22.46	2.034e-16	161.10	<0.025	<0.051
C-UVLG-23	149.88934	2.73473	27	0.709	21.41	8.128e-19	203.56	<0.019	<0.040
C-UVLG-24	150.17247	2.63495	108	0.752	22.43	1.660e-16	36.05	<0.111	<0.228
C-UVLG-25	149.62904	1.66577	81	0.671	22.02	1.182e-20	74.98	<0.053	<0.109
C-UVLG-26	149.60760	2.16737	108	0.676	22.28	6.302e-19	121.33	<0.033	<0.068
C-UVLG-27	149.69514	2.74294	108	0.652	22.52	1.015e-19	82.99	<0.048	<0.099
C-UVLG-28	150.45580	1.65284	81	0.657	22.66	4.344e-19	33.84	<0.118	<0.243
C-UVLG-29	149.46870	2.58616	81	0.704	21.94	1.005e-18	66.43	<0.060	<0.124
C-UVLG-30	149.51488	1.89228	108	0.694	22.56	8.146e-17	50.50	<0.079	<0.163
C-UVLG-33	150.76311	2.80412	108	0.693	22.37	3.299e-19	124.97	<0.032	<0.065
C-UVLG-34	150.69376	2.84451	108	0.738	22.68	8.607e-17	62.97	<0.063	<0.130
C-UVLG-35	149.69348	2.59921	27	0.678	21.35	1.490e-18	72.07	<0.055	<0.114
Stack (18 Galaxies)				0.685	22.14	378.7	<0.011	<0.022	
Stack (8 Galaxy Mergers)				0.678	22.50	223.2	<0.018	<0.037	

NOTE. — The values presents are 3σ limits. Objects 3, 9, 10, 13, 14, 16, 22, 31 and 32 were not detected in the FUV direct image, target 17 was an AGN

^aNUV magnitude from GALEX public release ver. 3

^bin units of $\text{ergs/s/cm}^2/\text{\AA}$

^cassumes and intrinsic flux ratio of $(f_{1500}/f_{830})_{int} = 3.4$ based in part from (Steidel et al. 2001)

^dassumes $(f_{1500}/f_{830})_{int} = 7$ (Siana et al. 2007)

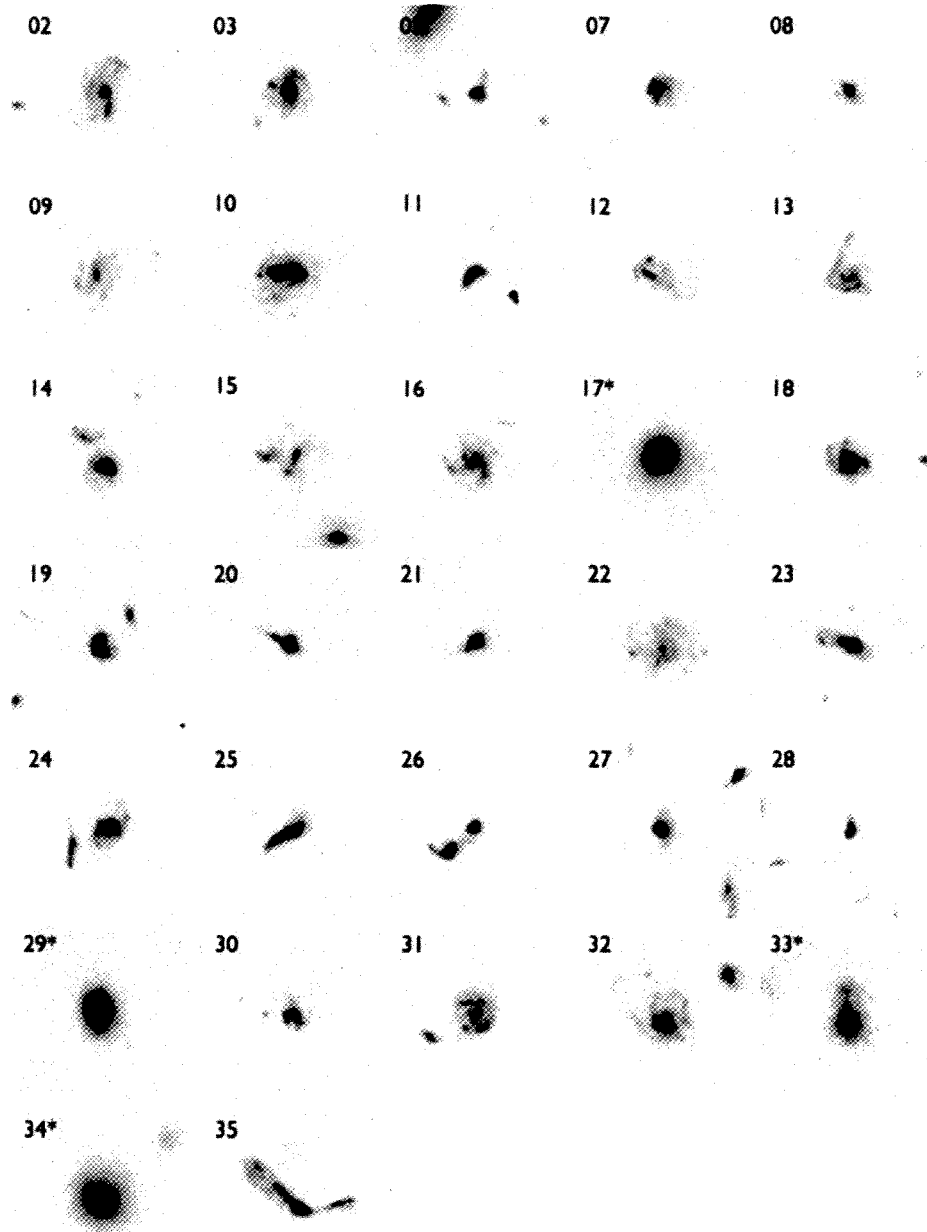


FIG. 2.— Optical images of the 32 $z \sim 0.7$ LBG analogs. Thumbnails are F814W *HST* images except those marked with an asterisk (#17, 29, 33, 34) which are CFHT ground-base i' . The images are 7'' on a side, with the object ID noted in the left corner.

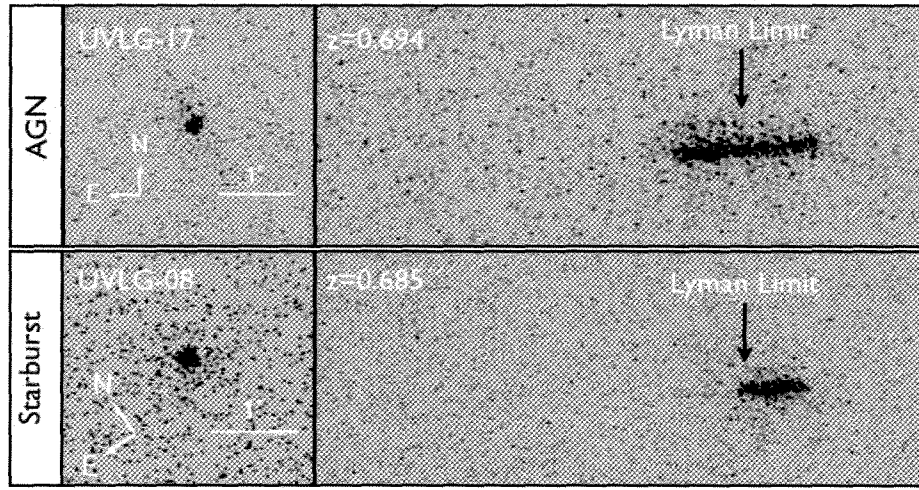


FIG. 3.— Example of the SBC F150LP direct UV image (left) and two-dimensional spectra (right) of an AGN (UVLG-17) and a starburst galaxy (UVLG-08) in our sample. The Lyman limit is noted in each spectra. Flux below 912Å is clearly detected in the AGN, while no LyC detection is found in the starburst galaxy. Wavelength increases from the left to right covering $\sim 1220\text{\AA}$ - 2000\AA observed.

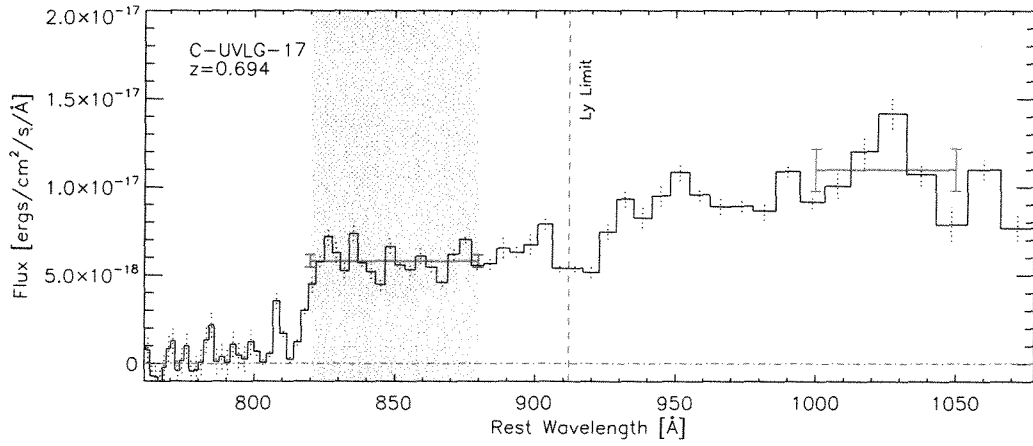
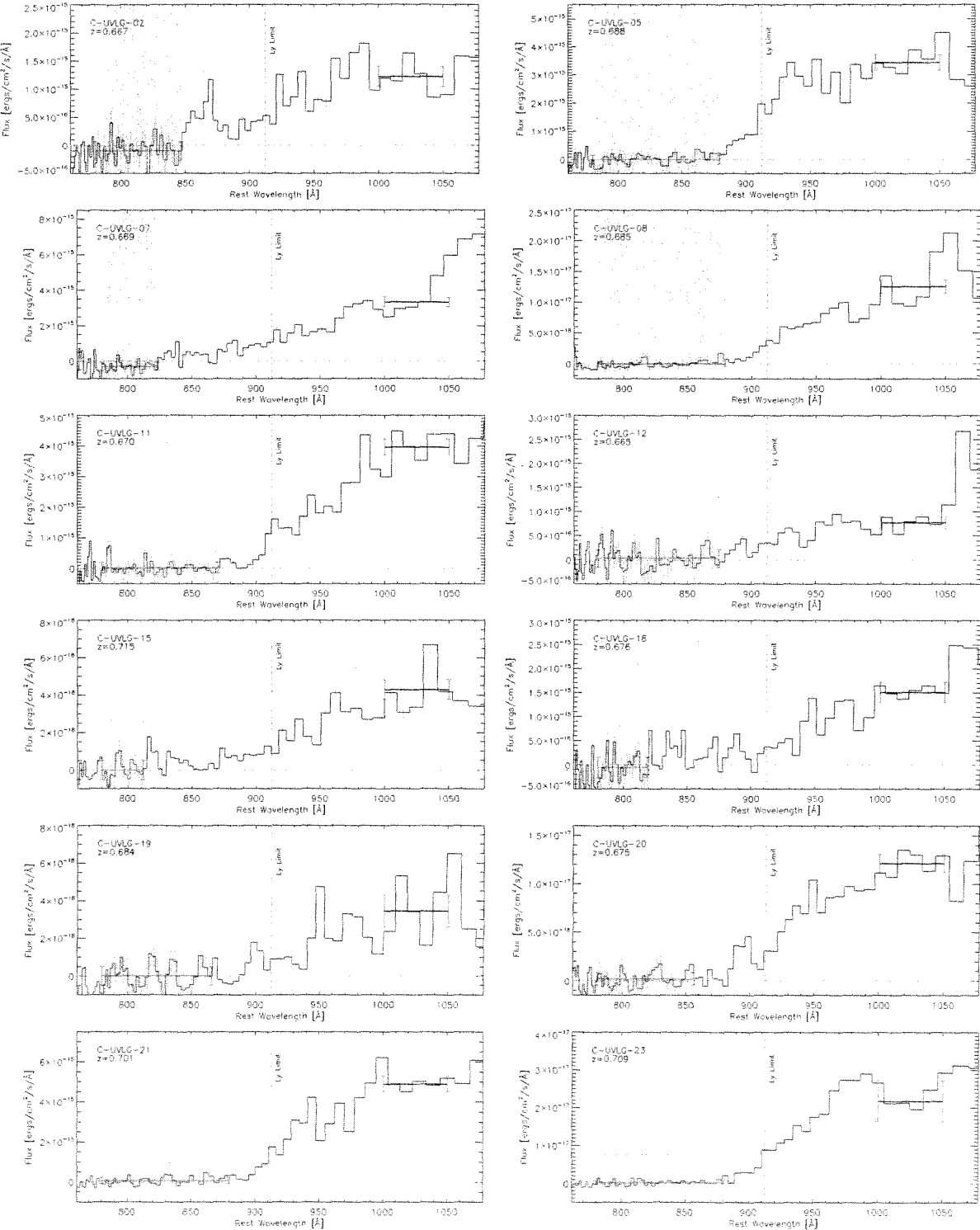
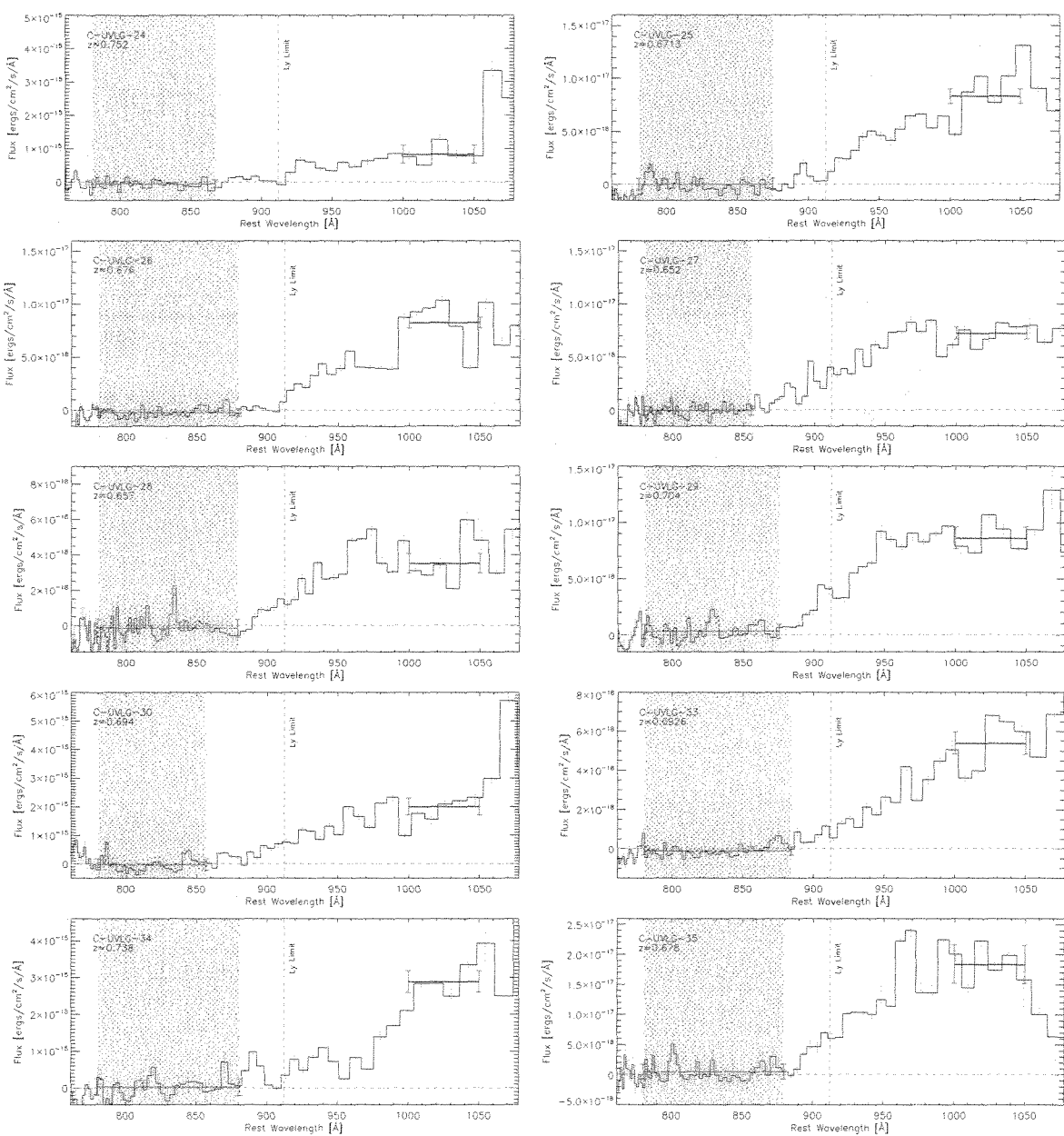


FIG. 4.— The individual spectrum of galaxy C-UVLG-17. Below the Lyman limit UV flux is clearly detected, showing that if LyC photons were escaping at the $\sim 15\%$ level it would be detected by our observations. The source of these photons is likely the Type 2 AGN.

FIG. 5.— Deep UV slitless spectra of $z \sim 0.7$ LBG analogs in the COSMOS field. The spectra have been shifted into the rest frame and fluxes are in $\text{ergs}/\text{cm}^2/\text{s}/\text{\AA}$. The horizontal lines (red) represent the average flux over two wavelength ranges, $\sim 780\text{-}880\text{\AA}$ and $1000\text{-}1050\text{\AA}$ with 3σ error bars.





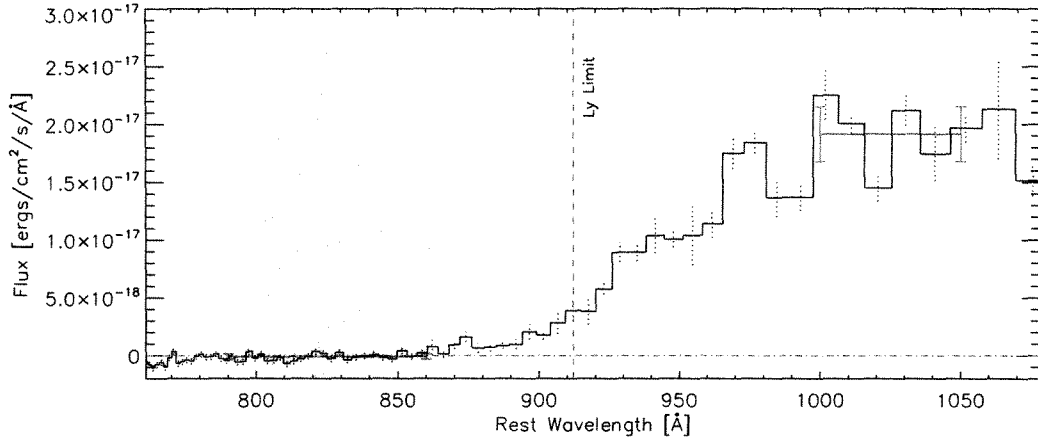


FIG. 6.— The stacked spectrum of 18 $z \sim 0.7$ LBG analogs. The 3σ upper limits on the observed UV-to-LyC flux density ratio is 378.7. Assuming an intrinsic Lyman break of 3.4 the upper limit on the *relative* escape fraction is 0.01 (3σ). The Lyman limit is indicated by the vertical dashed line. The horizontal lines (red) represent the average LyC and f_{1025} flux used to derive the escape fraction. Error bars are discussed in section 3.1 and are the same as in Figure 7

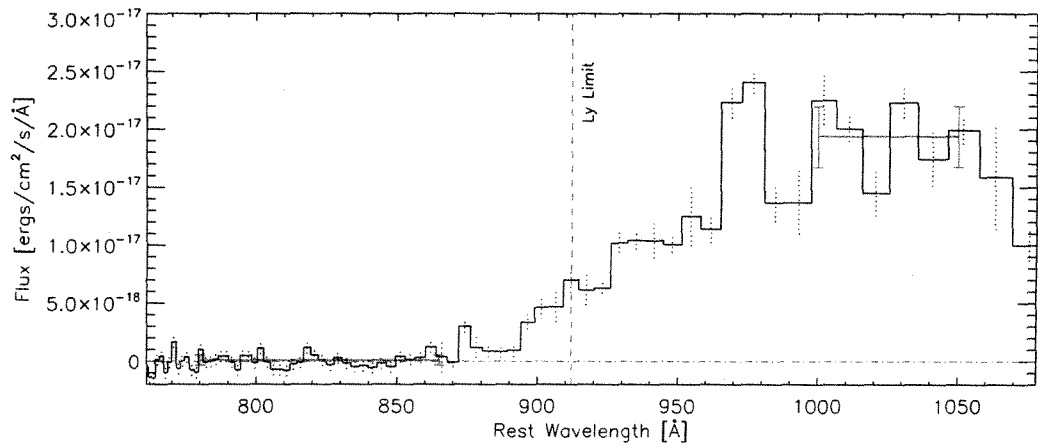


FIG. 7.— The stacked spectrum of 8 $z \sim 0.7$ LBG analogs with a merger morphology. The 3σ upper limits on the observed UV-to-LyC flux density ratio is 223.2. Assuming an intrinsic Lyman break of 3 the relative escape fraction is 0.02 (3σ). The Lyman limit is indicated by the vertical dashed line. The horizontal lines (red) represent the average flux over two wavelength ranges, 800–860Å and 1000–1050Å with 3σ error bars.

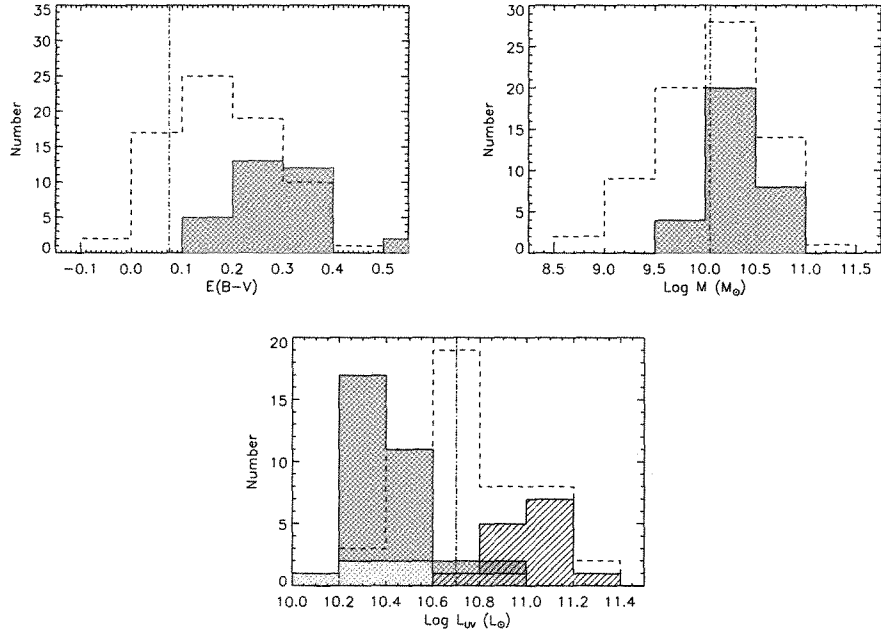


FIG. 8.— Histograms of extinction (left), stellar mass (right) and rest-frame UV luminosity (bottom) for the 32 local LBG analogs. The darker shaded regions highlight the 32 galaxies presented in this paper. A sample of $z \sim 3$ LBGs (dashed lines) in all three panels are taken from Shapley et al. (2005). The dash-dotted vertical lines show the average extinction (Verma et al. 2007), and stellar mass (Yan et al. 2006) for $z \gtrsim 5$ galaxies and the typical L_* for $z \sim 6$ galaxies (Bouwens et al. 2006). (Bottom) The 7 direct detections of LyC flux in LBGs reported in Iwata et al. (2008) are denoted by the lighter shaded histogram, and the lined (angled) histogram shows the $z \sim 3$ LBG sample of Shapley et al. (2006). The extinction and stellar mass for the COSMOS sources were estimated in the photometric redshift fitting (Mobasher et al. 2007), and the UV luminosity from the GALEX NUV (Zamojski et al. 2007). The histograms show that the galaxies presented in this paper have low levels of extinction, similar stellar masses and rest-frame UV luminosities compared to $z \sim 3$ LBGs.

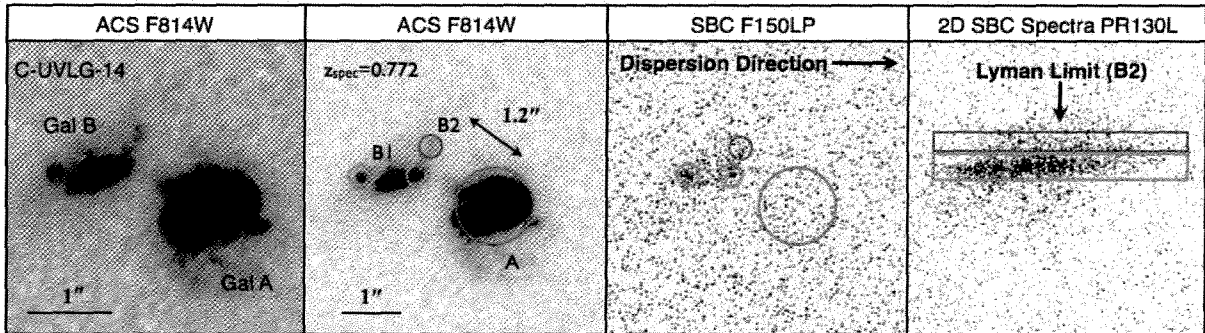


FIG. 9.— Postage stamp images left to right are: *HST* F814W zoomed in followed by F814W, SBC FUV F150LP and the FUV 2D spectra. Galaxy A (GalA) and Galaxy B (GalB) are noted in the images. The FUV flux and sites of escaping LyC are concentrated in knots (highlighted by circles) in GalB and are referred to in the text as GalB1 and GalB2. The merging pair is separated by ~ 10 kpc on the sky. Boxes approximate the extraction regions of the UV spectra in the 2D spectral image. Flux below the Lyman limit (assuming a $z=0.772$) is seen to the right of the arrow.

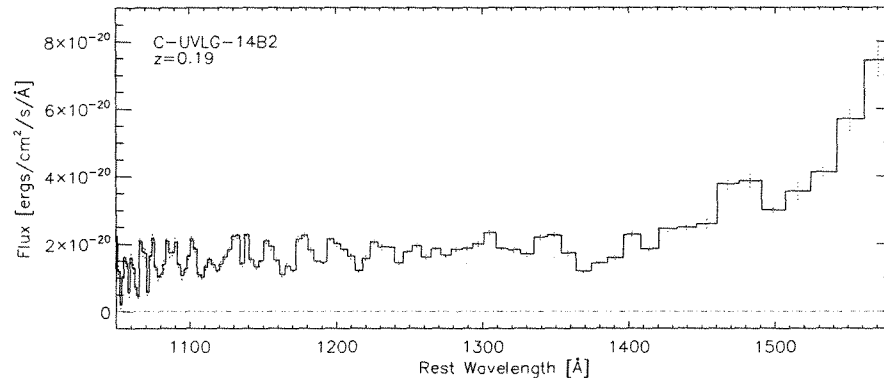


FIG. 10.— One-dimensional rest-frame UV spectra of GalB2, a low redshift interloper at $z=0.19$.